PROCEEDINGS A

royalsocietypublishing.org/journal/rspa

Research

Cite this article: Neukirch S, Audoly B. 2021 A convenient formulation of Sadowsky's model for elastic ribbons. *Proc. R. Soc. A* **477**: 20210548.
https://doi.org/10.1098/rspa.2021.0548

Received: 6 July 2021
Accepted: 20 October 2021

Subject Areas:
mechanical engineering, structural engineering, applied mathematics

Keywords:
boundary value problems, elastic plates, twisted rods

Author for correspondence:
Sébastien Neukirch
e-mail: sebastien.neukirch@sorbonne-universite.fr

Electronic supplementary material is available online at https://doi.org/10.6084/m9.figshare.c.5705318.

THE ROYAL SOCIETY PUBLISHING

Downloaded from https://royalsocietypublishing.org/ on 17 November 2021

A convenient formulation of Sadowsky's model for elastic ribbons

Sébastien Neukirch[1] and Basile Audoly[2]

[1]D'Alembert Institute for Mechanics, CNRS and Sorbonne Université, Paris UMR 7190, France
[2]Laboratoire de Mécanique des Solides, CNRS, Institut Polytechnique de Paris, Palaiseau 91120, France

Elastic ribbons are elastic structures whose length-to-width and width-to-thickness aspect ratios are both large. Sadowsky proposed a one-dimensional model for ribbons featuring a nonlinear constitutive relation for bending and twisting: it brings in both rich behaviours and numerical difficulties. By discarding non-physical solutions to this constitutive relation, we show that it can be inverted; this simplifies the system of differential equations governing the equilibrium of ribbons. Based on the inverted form, we propose a natural regularization of the constitutive law that eases the treatment of singularities often encountered in ribbons. We illustrate the approach with the classical problem of the equilibrium of a Möbius ribbon, and compare our findings with the predictions of the Wunderlich model. Overall, our approach provides a simple method for simulating the statics and the dynamics of elastic ribbons.

1. Introduction

Analysing the equilibrium of elastic ribbons is somewhat simpler than that of elastic plates, but ribbons inherit some of the difficulties present in elastic plates theory. One of these difficulties is the stress concentration caused by the near-inextensibility of the plate mid-surface, as found for instance in the Möbius configuration of an elastic ribbon.

In 1858, A. F. Möbius introduced its celebrated one-sided surface: a ribbon twisted and closed in such a way that its edge is a single curve. Although the Möbius strip was originally introduced as a topological curiosity, it has given rise to a challenge in elasticity theory: What is the equilibrium shape of a Möbius band made out of an elastic material? The energy

© 2021 The Author(s) Published by the Royal Society. All rights reserved.

Downloaded from https://royalsocietypublishing.org/ on 17 November 2021

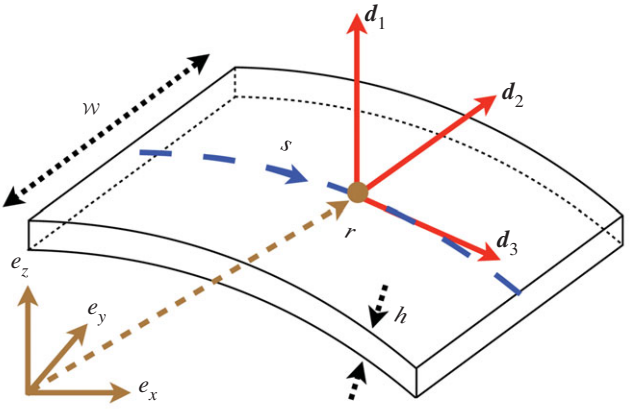

Figure 1. A ribbon with width w, thickness h is seen as a one-dimensional elastic structure with centre-line $\boldsymbol{r}(s)$ and Cosserat local frame $\{\boldsymbol{d}_1(s), \boldsymbol{d}_2(s), \boldsymbol{d}_3(s)\}$, parametrized with the arc-length s. (Online version in colour.)

functional governing the equilibrium of such an elastic ribbon, in the narrow limit, has been introduced in [1], but it is only relatively recently that tractable equations for the minimization of the energy have been derived, and solved numerically, in [2]. This work initiated a surge of interest from the applied mathematics community, see for example the book edited in [3].

Two main difficulties arise when solving the equilibrium equations for ribbons numerically: (i) they are differential algebraic equations (DAEs) and (ii) singularities are often present in their solution. In general, DAE systems are more difficult to solve than ordinary differential equations (ODEs) and numerical integrators are less commonly found, and typically less optimized. Singularities in the solutions are encountered in the Möbius problem as well as in other geometries: they typically require the integration interval to be arranged (and sometimes broken down) manually in such a way that the singularities lie at their endpoints, as done in past analyses of the Möbius problem [4,5].

In this paper, we address both these problems and propose a variant of the Sadowsky model for thin elastic ribbons that takes the form of an ODE and is regularized by a small parameter.

2. Equilibrium of elastic ribbons (Sadowsky's model)

We consider an elastic structure having length L, width w and thickness h with $L \gg w \gg h$; see figure 1. It is made of a linearly elastic, isotropic material with Young's modulus E and Poisson's ratio ν. Its deformations are computed with a one-dimensional model based on the plate bending rigidity $D = Eh^3/(12(1-\nu^2))$. We work in the *special* set of units where $Dw = 1$ and $L = 1$. The extension to a *generic* set of units involves restoring the appropriate factors Dw and L in our formulas, as found by a standard scaling analysis.

The Sadowsky model for thin, inextensible ribbons is a one-dimensional theory that is formulated as follows [1,2,6]. We denote as s the arc-length in reference configuration; it is used as a Lagrangian coordinate that follows material cross sections. In actual configuration, the main unknowns are the centre-line $\boldsymbol{r}(s)$ of the structure and a set of three orthonormal vectors $\{\boldsymbol{d}_1(s), \boldsymbol{d}_2(s), \boldsymbol{d}_3(s)\}$ that capture how the cross section twists about the centre-line. The combination of a centre-line and a set of directors defines a so-called Cosserat rod model. Effectively, the one-dimensional model is such that the centre-line is inextensible and unshearable, implying the following kinematic constraint

$$\boldsymbol{r}'(s) = \boldsymbol{d}_3(s). \tag{2.1}$$

royalsocietypublishing.org/journal/rspa Proc. R. Soc. A 477: 20210548

Downloaded from https://royalsocietypublishing.org/ on 17 November 2021

The evolution of the Cosserat orthonormal frame as s is varied and is given by the Darboux equation

$$\boldsymbol{d}_i'(s) = \boldsymbol{u}(s) \times \boldsymbol{d}_i(s) \quad \text{with } 1 \le i \le 3, \tag{2.2}$$

with $\boldsymbol{u}(s)$ as the Darboux vector and $f'(s) = \mathrm{d}f/\mathrm{d}s$ as the derivative of a generic function $f(s)$ along the centre-line. Here, the existence and unicity of $\boldsymbol{u}(s)$ follows from the orthonormal character of the frame of directors $\boldsymbol{d}_i(s)$ for any s. We work with the components $\{u_1(s), u_2(s), u_3(s)\}$ of the Darboux vector in the directors frame,

$$u_i(s) = \boldsymbol{u}(s) \cdot \boldsymbol{d}_i(s).$$

These $u_i(s)$ are the strain measures of the rod model, for bending ($i = 1, 2$) and twisting ($i = 3$).

Let us now turn to the analysis of stress in the ribbon. We denote as $\boldsymbol{n}(s)$ the force arising from the internal stress transmitted across an imaginary cut made along the cross section with coordinate s and $\boldsymbol{m}(s)$ the resultant moment: $\boldsymbol{n}(s)$ and $\boldsymbol{m}(s)$ are the internal force and moment, respectively. We limit attention to ribbons made of a uniform elastic material, with uniform cross-section geometry in the longitudinal direction. The constitutive relations connecting the bending and twisting strains $u_i(s)$ with the components $m_i(s) = \boldsymbol{m}(s) \cdot \boldsymbol{d}_i(s)$ of the internal moment in the directors basis write

$$u_1(s) = 0 \tag{2.3}$$

$$m_2(s) = u_2 \left(1 - \frac{u_3^4}{u_2^4}\right) \tag{2.4}$$

and

$$m_3(s) = 2\, u_3 \left(1 + \frac{u_3^2}{u_2^2}\right). \tag{2.5}$$

Note that these constitutive relations are nonlinear, and that the stress m_1 is absent from the first one: equation (2.3) is a constitutive *constraint* expressing the fact that the elastic modulus associated with bending the ribbon in its own plane is much larger than for the other bending mode.

The set of equations governing the equilibrium of the ribbon is complemented with the Kirchhoff equations for the balance of force and moment,

$$\boldsymbol{n}'(s) = \boldsymbol{0} \tag{2.6}$$

and

$$\boldsymbol{m}'(s) + \boldsymbol{r}'(s) \times \boldsymbol{n}(s) = \boldsymbol{0}. \tag{2.7}$$

We do not consider any distributed force or moment, such as gravity or contact forces.

The equilibrium of the ribbon can be found by solving equations (2.1)–(2.7) with the appropriate conditions on the boundaries $s = 0$ and $s = 1$.

The equilibrium problems (2.1)–(2.7) can be derived variationally from the constitutive constraint $u_1(s) = 0$ in (2.3) and from the strain energy functional

$$W_S(u_2, u_3) = \frac{1}{2}\left(u_2^2 + 2\, u_3^2 + \frac{u_3^4}{u_2^2}\right), \tag{2.8}$$

which is such that the constitutive relations (2.4) and (2.5) can be rewritten as $m_i(s) = (\partial W_S/\partial u_i)(u_2(s), u_3(s))$ for $i = 2, 3$. This variational derivation first appeared in [2]; a presentation fully in line with the theory of nonlinear elastic rods was later proposed in [6].

The classical Kirchhoff rod model is recovered by changing the constitutive relations (2.3)–(2.5) to $m_i(s) = B_i\, u_i(s)$, for $1 \le i \le 3$. Contrary to the case of ribbons, these constitutive relations are linear. The elastic constants B_i are the bending ($1 \le i \le 2$) and twisting rigidities ($i = 3$) of the rod. A rod with Young's modulus E, shear modulus $G = E/(2(1+\nu))$ and a rectangular cross section (width w, thickness h) has $B_1 = E\, h\, w^3/12$, $B_2 = E\, h^3\, w/12$ and $B_3 = G\, h^3\, w/3$, in the limit $w \gg h$.

Downloaded from https://royalsocietypublishing.org/ on 17 November 2021

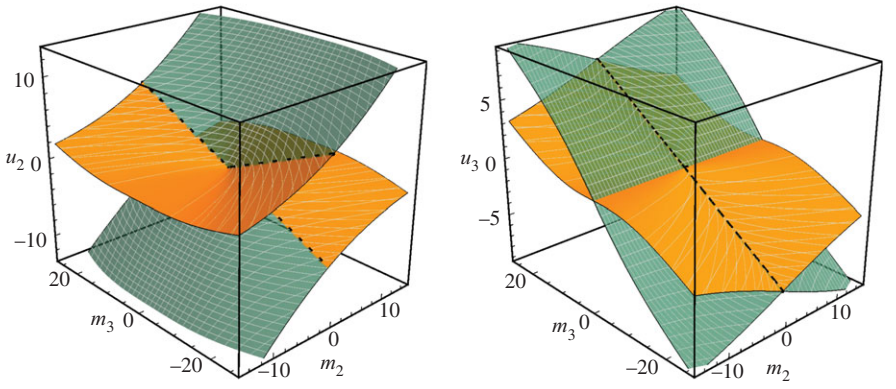

Figure 2. Inverting Sadowsky's constitutive relations. The surfaces are generated as parametric plots using the bending and twisting strain (u_2, u_3) as parameters. The bending and twisting moments (m_2, m_3) on the horizontal axes are calculated from the constitutive relation (2.4) and (2.5). The bending and twisting strains (u_2, u_3) are used on either one of the vertical axes. The surface is coloured in green if $|\eta| < 1$ and in orange if $|\eta| > 1$, with $\eta = u_3/u_2$. The presence of two sheets stacked vertically shows that it is impossible to invert the constitutive law as $u_2 = g_2^{-1}(m_2, m_3)$ and $u_3 = g_3^{-1}(m_2, m_3)$ in general. However, this inversion becomes possible if the condition $|\eta| < 1$ is enforced, as shown by the layout of the green sections of the sheets. (Online version in colour.)

3. Equilibrium as a differential algebraic system

The equations for the statics of ribbons derived in §2 form a nonlinear boundary-value problem with the arc-length s as independent variable, i.e. a set of differential equations with boundary conditions at both endpoints $s = 0$ and $s = 1$.

Specifically, equations (2.1)–(2.7) can be written as a differential system for six unknown vectors $\boldsymbol{\theta}_1 = (\boldsymbol{r}, \boldsymbol{d_1}, \boldsymbol{d_2}, \boldsymbol{d}_3, \boldsymbol{n}, \boldsymbol{m})$ plus two unknown scalars $\boldsymbol{\theta}_2 = (u_2, u_3)$ as

$$\begin{pmatrix} \boldsymbol{r} \\ \boldsymbol{d}_i \\ \boldsymbol{n} \\ \boldsymbol{m} \end{pmatrix}' = \begin{pmatrix} \boldsymbol{d}_3 \\ (u_2\,\boldsymbol{d}_2 + u_3\,\boldsymbol{d}_3) \times \boldsymbol{d}_i \\ \boldsymbol{0} \\ \boldsymbol{n} \times \boldsymbol{d}_3 \end{pmatrix} \Longleftrightarrow \boldsymbol{\theta}_1' = \boldsymbol{f}(\boldsymbol{\theta}_1, \boldsymbol{\theta}_2) \tag{3.1a}$$

and

$$\boldsymbol{0} = \begin{pmatrix} \dfrac{\partial W_S}{\partial u_2}(u_2, u_3) - \boldsymbol{m} \cdot \boldsymbol{d}_2 \\ \dfrac{\partial W_S}{\partial u_3}(u_2, u_3) - \boldsymbol{m} \cdot \boldsymbol{d}_3 \end{pmatrix} \Longleftrightarrow \boldsymbol{0} = \boldsymbol{g}(\boldsymbol{\theta}_1, \boldsymbol{\theta}_2). \tag{3.1b}$$

Due to the presence of the constraint $\boldsymbol{g}(\boldsymbol{\theta}_1, \boldsymbol{\theta}_2) = \boldsymbol{0}$, this problem is known as a DAE problem; the component form of this DAE is spelled out in appendix A.

A difficulty is that the constitutive relation $\boldsymbol{g}(\boldsymbol{\theta}_1, \boldsymbol{\theta}_2) = \boldsymbol{0}$ is nonlinear and *cannot* be inverted as $\boldsymbol{\theta}_2 = \boldsymbol{g}^{-1}(\boldsymbol{\theta}_1) \Leftrightarrow u_2 = g_2^{-1}(m_2, m_3)$ and $u_3 = g_3^{-1}(m_2, m_3)$. This prevents from rewriting (3.1) as an ODE $\boldsymbol{\theta}_1' = \boldsymbol{f}(\boldsymbol{\theta}_1, \boldsymbol{g}^{-1}(\boldsymbol{\theta}_1))$. By contrast, for classical elastic rods (Kirchhoff rod model), the *linear* constitutive relation $\boldsymbol{g}(\boldsymbol{\theta}_1, \boldsymbol{\theta}_2) = \boldsymbol{0}$ *can be* inverted as $u_2 = g_2^{-1}(m_2, m_3) := m_2/B_2$ and $u_3 = g_3^{-1}(m_2, m_3) := m_3/B_3$, implying that equilibrium can be rewritten as an ODE with $3 \times 6 = 18$ unknowns.

For thin ribbons, the impossibility to invert the constitutive relation as $u_2 = g_2^{-1}(m_2, m_3)$ and $u_3 = g_3^{-1}(m_2, m_3)$ is demonstrated graphically in figure 2. This is confirmed by the calculation from appendix B, where an attempt to invert the constitutive relations leads to multi-valued 'functions' $g_2^{-1}(m_2, m_3)$ and $g_3^{-1}(m_2, m_3)$, and therefore fails.

Downloaded from https://royalsocietypublishing.org/ on 17 November 2021

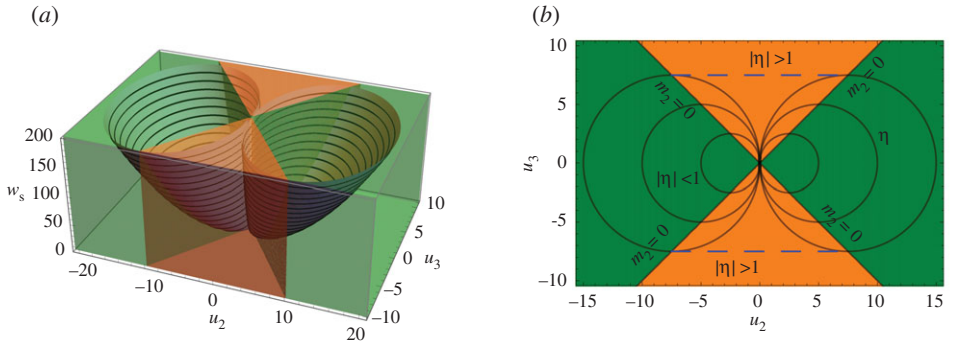

Figure 3. Sadowsky's energy surface $W_S(u_2, u_3)$ from equation (2.8). The energy surface is made up of two symmetric wells. Level sets are shown in black, and the 'forbidden' region corresponding to $|\eta| = |u_3/u_2| > 1$ is shaded in orange (see §4). (*a*) Three-dimensional plot. (*b*) Contour plot, with a level set of the convexified functional from [10] shown in dashed blue. (Online version in colour.)

Numerically, the standard method for dealing with the DAE system (3.1) is to augment the differential equation $\boldsymbol{\theta}_1' = \boldsymbol{f}(\boldsymbol{\theta}_1, \boldsymbol{\theta}_2)$ with the differentiated form of the constraint $\boldsymbol{g} = \boldsymbol{0}$, namely $(\partial \boldsymbol{g}/\partial \boldsymbol{\theta}_2) \cdot \boldsymbol{\theta}_2' = -(\partial \boldsymbol{g}/\partial \boldsymbol{\theta}_1) \cdot \boldsymbol{\theta}_1'$, resulting in an ODE with $3 \times 6 + 2 = 20$ unknowns. This is the approach chosen by several authors, see for example [7–9]. The drawback is that the resulting equations are complex; in the present work we explore a simpler approach based on the remark that the constitutive law becomes invertible when non-physical values of the strain are dismissed.

4. Inverting the constitutive law

The Sadowsky energy W_S in (2.8) is non-convex. As noted in [10], equations (2.1)–(2.7) are therefore not sufficient to warrant equilibrium. It must be required in addition that the solution lives in the region of the strain space where the solution is convex. The latter can be worked out as [10]

$$|\eta(s)| \leq 1 \quad \text{where } \eta(s) = \frac{u_3(s)}{u_2(s)}. \tag{4.1}$$

In the figures, we use the colour code of green for $|\eta(s)| \leq 1$ and orange for the 'forbidden' region $|\eta| > 1$.

A microscopic interpretation of the condition (4.1) can be found in [11], and a related discussion in the context of extensible ribbons is given in §7 of [12]. Note that the condition (4.1) amounts to replacing the Sadowsky energy W_S in equation (2.8) with the convexified energy W_F that matches W_S for $|\eta| \leq 1$ and is equal to $W_F(u_2, u_3) = 2\,u_3^2$ for $|\eta| \geq 1$ [10]; as shown in figure 3, the level sets of W_F coincide with those of W_S in the allowed region $|\eta| \leq 1$ but differ in the 'forbidden' region $|\eta| > 1$ (dashed blue segments in figure 3). We note that having $|\eta| > 1$ would mean obtaining a negative curvature u_2 with a positive applied bending moment m_2.

As shown in figure 2, it is possible to invert the constitutive law if one limits attention to the green portions of the surfaces, where the condition $|\eta| \leq 1$ holds. Closed-form expressions for the inverse constitutive law $u_2 = u_2^\star(m_2, m_3)$ and $u_3 = u_3^\star(m_2, m_3)$ are obtained as follows. We start by introducing $\lambda = \eta^2 = (u_3/u_2)^2$ and $a = m_2/m_3$. Expressing a using equations (2.4) and (2.5), we obtain $2\,a\eta = 1 - \lambda$. Squaring both sides of this equation yields $\lambda^2 - 2\,\lambda\,(2\,a^2 + 1) + 1 = 0$. This equation has two real and positive roots $\lambda^\star$ and $\lambda^{\star\star}$, which are such that $0 < \lambda^\star \leq 1 \leq \lambda^{\star\star}$. The condition $|\eta| \leq 1$ implies $\lambda = \eta^2 \leq 1$ and shows that the correct root is $\lambda^\star$. This yields, after some algebra

$$\lambda^\star(m_2, m_3) = 1 + 2\,a^2 - 2\sqrt{a^4 + a^2} \quad \text{with } a = \frac{m_2}{m_3} \tag{4.2}$$

Downloaded from https://royalsocietypublishing.org/ on 17 November 2021

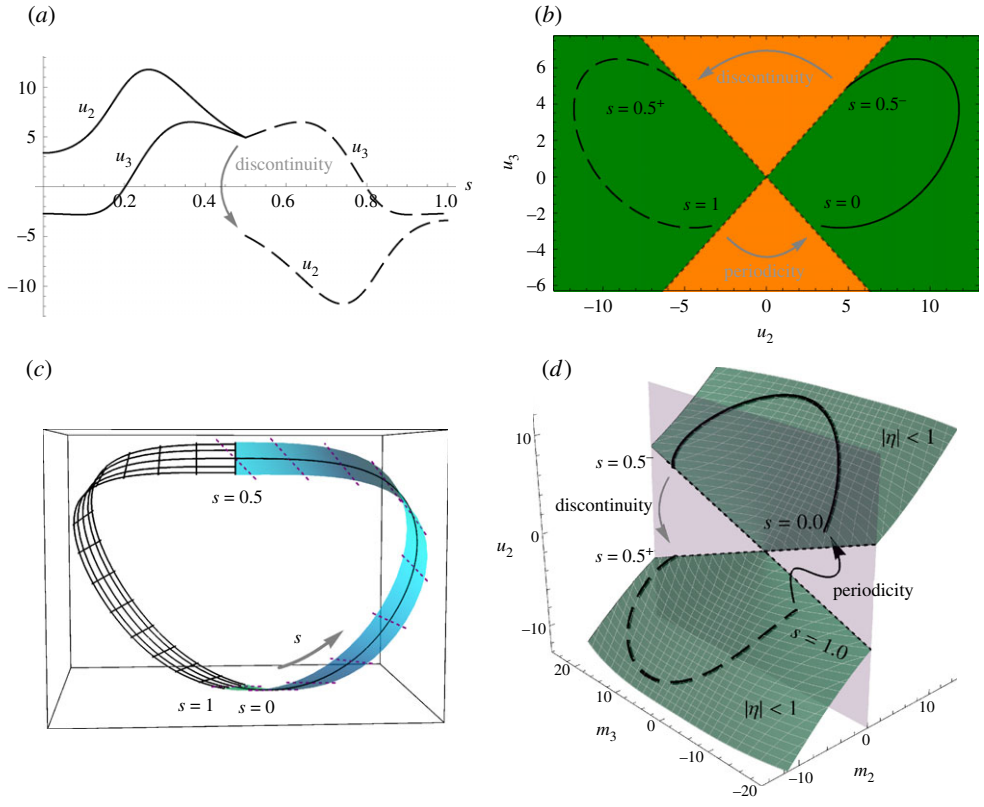

Figure 4. Möbius solution predicted by Sadowsky's model. The solution is only computed for $s \in (0; 1/2)$ (plain curves), and symmetry is used to plot the $s \in (1/2; 1)$ domain (dashed curves). (*a*) At the discontinuity $s = 1/2$, the curvature strain $u_2(s)$ changes sign, while the twisting strain $u_3(s)$ is continuous. (*b*) Parametric plot in the (u_2, u_3) plane, showing that the solution lies entirely in the region $\eta(s) \leq 1$ (green background). (*c*) Three-dimensional rendering of the Möbius solution, including the generatrices (dotted lines). (*d*) The parametric plot of the solution in the (m_2, m_3, u_2) space falls on the green surface predicted by the inverse constitutive law (4.3). (Online version in colour.)

$$u_2^\star(m_2, m_3) = \frac{m_2}{(1-\lambda^\star)(1+\lambda^\star)} \tag{4.3}$$

and

$$u_3^\star(m_2, m_3) = \frac{m_3}{2(1+\lambda^\star)}. \tag{4.4}$$

Note the existence of a discontinuity in $u_2^\star(m_2, m_3)$ at $m_2 = 0$ when $m_3 \neq 0$, which corresponds to crossing the forbidden region shown in orange in the figures. The inverse constitutive law (4.3) and (4.4) yields the green surface shown in figure 4, which coincides with the green portions appearing in figure 2. It covers the first and third alternatives in equation (6.8) of [13].

Using the inverse constitutive law (4.2)–(4.4), it is now possible to eliminate u_2 and u_3 from the differential system (3.1), which then takes the form of an ODE,

$$\begin{pmatrix} \boldsymbol{r} \\ \boldsymbol{d}_i \\ \boldsymbol{n} \\ \boldsymbol{m} \end{pmatrix}' = \begin{pmatrix} \boldsymbol{d}_3 \\ (u_2^\star \boldsymbol{d}_2 + u_3^\star \boldsymbol{d}_3) \times \boldsymbol{d}_i \\ \boldsymbol{0} \\ \boldsymbol{n} \times \boldsymbol{d}_3 \end{pmatrix} \Longleftrightarrow \boldsymbol{\theta}_1' = \boldsymbol{f}^\star(\boldsymbol{\theta}_1). \tag{4.5}$$

The order of the differential equation is 18.

By formally setting $\lambda^\star = 0$ in equations (4.3) and (4.4), one recovers the inverse constitutive laws $u_2^\star = m_2$ and $u_3^\star = m_3/2$ applicable to a classical Kirchhoff rod having $B_3/B_2 = 2$. By

Downloaded from https://royalsocietypublishing.org/ on 17 November 2021

introducing a homotopy coefficient ρ ($0 \le \rho \le 1$) and by replacing $\lambda^\star$ with $\rho\,\lambda^\star$ in equations (4.3) and (4.4), it is therefore possible to continuously change the constitutive law, from a Kirchhoff rod model with $B_1 = \infty$, $B_2 = 1$ and $B_3 = 2$ to Sadowsky's ribbon model, as shown in appendix C. This makes it possible to treat both the Sadowsky and Kirchhoff models using the same computer code.

5. Illustration: Möbius strip

We illustrate this approach by solving the equilibrium of a Möbius strip, i.e. a ribbon that is twisted by half a turn and closed into a loop. The differential equation $\boldsymbol{\theta}_1' = \boldsymbol{f}^\star(\boldsymbol{\theta}_1)$ in (4.5) is solved on the interval $0 \le s \le 1/2$, together with 18 scalar boundary conditions

$$\left.\begin{aligned} &\boldsymbol{r}(0) = \boldsymbol{0} \quad \boldsymbol{n}(0)\cdot\boldsymbol{d}_1(0) = 0 \quad \boldsymbol{m}(0)\cdot\boldsymbol{d}_1(0) = 0 \\ &\boldsymbol{d}_1(0) = \boldsymbol{e}_x \quad \boldsymbol{d}_2(0) = \boldsymbol{e}_y \quad \boldsymbol{d}_3(0) = \boldsymbol{e}_z \\ \text{and}\quad &\boldsymbol{r}\left(\frac{1}{2}\right)\cdot\boldsymbol{e}_i = 0\ (i = x, y) \quad \boldsymbol{d}_1\left(\frac{1}{2}\right)\cdot\boldsymbol{e}_x = 0 \quad \boldsymbol{d}_3\left(\frac{1}{2}\right)\cdot\boldsymbol{e}_x = 0. \end{aligned}\right\} \tag{5.1}$$

The boundary conditions at $s = 1/2$ reflect the flip-symmetric nature of the solution, as assumed in previous works [2,4,14,15]. A simple shooting procedure, presented in the electronic supplementary material, yields the components of $\boldsymbol{n}(0)$ and $\boldsymbol{m}(0)$ in the Cartesian frame as $(n_x(0), n_y(0), n_z(0)) = (0, 43.5, 42.1)$ and $(m_x(0), m_y(0), m_z(0)) = (0, 2.01, -8.87)$, as well as a solution on the interval $0 \le s \le 1/2$. The solution on the other interval $1/2 \le s' \le 1$ is then generated by symmetry, using $u_2(s') = -u_2(1 - s')$ and $u_3(s') = +u_3(1 - s')$.

In figure 4*a*, the solutions $u_2(s)$ and $u_3(s)$ are plotted. The point $s = 1/2$ is a discontinuity where u_2 flips sign while u_3 remains continuous. At the discontinuity, $|u_2((1/2)^\pm)| = |u_3(1/2)|$, implying that $\eta(s)$ jumps from $+1$ at $s = (1/2)^-$ to -1 at $s = (1/2)^+$. In the space (u_2, u_3) shown in figure 4*b*, the discontinuity causes a jump across the forbidden region, as shown by the grey arrow. In the space (m_2, m_3, u_2) it causes a jump from one green sheet to the other; see figure 4*d*. The equilibrium imposes that the components $m_2(s)$ and $m_3(s)$ of the internal moment are continuous at the discontinuity.

Let us now turn to the periodicity condition at the $s = 1$ endpoint. As the Möbius strip is not orientable, the directors $\boldsymbol{d}_1$ and $\boldsymbol{d}_2$ are opposite to each other there, $\boldsymbol{d}_i(1) = -\boldsymbol{d}_i(0)$ for $i = 1, 2$. Even although the Darboux vector $\boldsymbol{u}$ is continuous, $\boldsymbol{u}(1) = \boldsymbol{u}(0)$, the non-orientability creates an apparent jump in the bending and twisting strains $u_i(1) = -u_i(0)$ for $i = 1, 2$, materialized by the second arrow in figure 4*b*,*d*.

We have recovered the solution of the Möbius problem predicted by the Sadowsky model that appeared in previous works, using a simple, constraint-free formulation (4.5). The singularity $s = 1/2$ has been placed at an *endpoint* of the mathematical domain $s \in (0, 1/2)$ on which we solved the boundary-value problem (5.1). In this happy but somewhat peculiar situation, there is no discontinuity inside the simulation domain $(0, 1/2)$. In general, however, the solutions of Sadowsky's model may feature interior discontinuities, and they must be taken care of by means of special jump conditions; see [10] as well as §7 in [12]. Interior discontinuities may appear under various loading conditions, and have been reported in [16–18]. As the position of an interior discontinuity is not known *a priori* in the absence of symmetry, dealing with them requires additional work.

6. Smoothing discontinuities

In this section, we present a method that avoids dealing with interior discontinuities. We observe that the inverse constitutive law $u_2 = u_2^\star(m_2, m_3)$ in equation (4.3) can be regularized as follows:

$$u_2^\star(m_2, m_3, \varepsilon) = \frac{m_2}{(1 - \lambda^\star + \varepsilon)\,(1 + \lambda^\star)}. \tag{6.1}$$

Downloaded from https://royalsocietypublishing.org/ on 17 November 2021

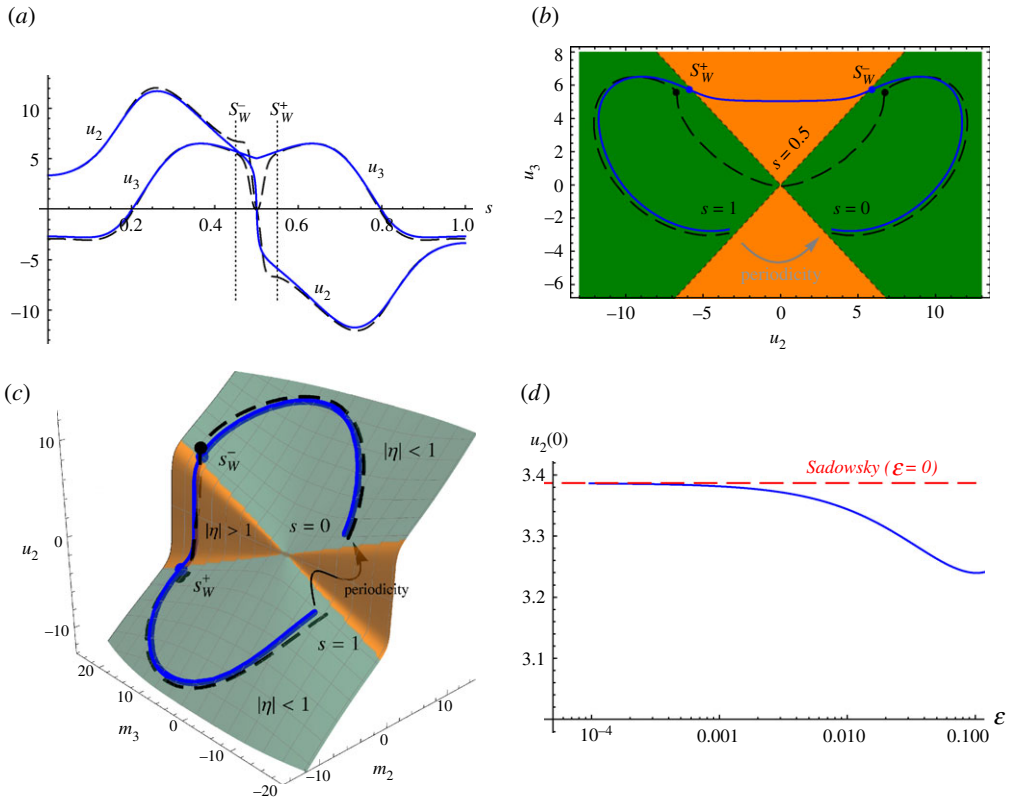

Figure 5. Solution of the regularized Sadowsky model from §6 for $\varepsilon = 0.01$ (solid blue curves) for a Möbius band, and comparison with the Wunderlich model (dashed black curves). The points $W^{\pm}$ are where the solution of the regularized Sadowsky model enters or exits the forbidden zone $|\eta| > 1$. (*a*) Bending and twisting strain, $u_i(s)$. (*b*) Parametric plot in the (u_2, u_3) plane. (*c*) Parametric plot in the (m_2, m_3, u_2) space, and comparison with the regularized constitutive law (6.1) (surface). (*d*) Convergence of the value $u_2(0)$ predicted by the regularized Sadowsky model (blue curve) to that predicted by the original Sadowsky model (red). The data for the Wunderlich solution are taken from [5]; see the green curve of their figure 7, with $w/L = 0.2/\pi$. (Online version in colour.)

We have introduced a small regularizing parameter $\varepsilon > 0$ in the denominator, such that the Sadowsky model is recovered in the limit $\varepsilon \to 0$. This regularization corresponds to going from the discontinuous surface shown in figure 4*c* to the smooth one shown in figure 5*c* for $\varepsilon = 0.01$. Note that this regularized constitutive law suppresses interior discontinuities, but puts an end to the variational nature of the model.

For the Möbius problem, it is now possible to solve the differential system (4.5) on the *entire* interval $s \in (0, 1)$. Using the smoothed constitutive law (6.1) for u_2 and the original constitutive law (4.4) for u_3, together with the clamped boundary conditions

$$\left.\begin{aligned} &\boldsymbol{r}(0) = \boldsymbol{0} \quad \boldsymbol{d}_1(0) = \boldsymbol{e}_x \quad \boldsymbol{d}_2(0) = \boldsymbol{e}_y \quad \boldsymbol{d}_3(0) = \boldsymbol{e}_z \\ \text{and} \quad &\boldsymbol{r}(1) = \boldsymbol{0} \quad \boldsymbol{d}_1(1) \cdot \boldsymbol{d}_2(0) = 0 \quad \boldsymbol{d}_2(1) \cdot \boldsymbol{d}_3(0) = 0 \quad \boldsymbol{d}_3(1) \cdot \boldsymbol{d}_1(0) = 0, \end{aligned}\right\} \tag{6.2}$$

we did obtain the solution of the regularized problem over the entire interval $s \in (0, 1)$ directly, by a shooting method. The initial values for $\varepsilon = 0.01$ were obtained numerically as $(n_x(0), n_y(0), n_z(0)) = (0, 43.1, 43.0)$ and $(m_x(0), m_y(0), m_z(0)) = (0, 2.15, -8.65)$. This solution is shown by the solid blue curves in figure 5. Details of the numerical solution are provided in the electronic supplementary material.

Downloaded from https://royalsocietypublishing.org/ on 17 November 2021

Note that the equilibrium equations (2.7), together with the periodic conditions for $\boldsymbol{r}(s)$ in (6.2), suffice to warrant that both $\boldsymbol{n}(s)$ and $\boldsymbol{m}(s)$ are periodic. Replacing the condition $x(1) = 0$ with $n_1(0) = 0$ helps the numerical resolution of the BVP by removing its s invariance.

The convergence of the solution of the regularized problem towards the solution of the original Sadowsky problem for $\varepsilon \to 0$ is checked in figure 5*d*, where the value of $u_2(0)$ is plotted as a function of ε. The limiting value $u^0_{2,S} = 3.3866$ predicted by the original Sadowsky model is recovered asymptotically for $\varepsilon \to 0$.

From figure 5*c*, it appears that the solution still switches from the upper green layer to the lower green layer across the mid-point $s = 1/2$, but this transition now takes place smoothly. As shown in figure 5*b*, the regularized solution does enter the region $|\eta| > 1$ that was forbidden in the original Sadowsky model, near the smoothed discontinuity $s = 1/2$.

In figure 5, this solution is also compared with the solution of the more accurate—but also numerically more challenging—Wunderlich model, governed by the functional

$$W_W(u_2, u_3) = W_S(u_2, u_3)\, \frac{1}{\eta' w}\, \log\left(\frac{2 + \eta' w}{2 - \eta' w}\right), \tag{6.3}$$

where $\eta(s) = u_3(s)/u_2(s)$ and with $w/L = 0.2/\pi$; see [19]. The Wunderlich energy W_W includes a gradient term $\eta'(s)$ that regularizes the discontinuities found in Sadowsky's model: the Wunderlich solutions feature an inner layer near $s = 1/2$. The detailed features of the inner layer of the Wunderlich solution are different from those of the regularized Sadowsky model, as shown by a comparison of the dashed black and solid blue curves near $s = 1/2$ (see, in particular, figure 5*b*). This could be expected from the fact that the Wunderlich model is designed to resolve the boundary layer accurately, the original Sadowsky model ignores it, and the regularized Sadowsky model provides a convenient but non-principled regularization. Still, the main point is that away from the smoothed discontinuity at $s = 1/2$, the solutions to the Sadowsky and Wunderlich models are similar [5,9]: this can be seen here by comparing figures 4 and 5.

7. Conserved quantities

We return to the original (non-regularized) Sadowsky model. Invariants have been extensively studied in Kirchhoff rods. In both Kirchhoff rods and ribbons that are free of any external load, the quantities $\boldsymbol{n}(s)$ and $\boldsymbol{n}(s) \cdot \boldsymbol{m}(s)$ are constant: this follows directly from the equations of equilibrium (2.6) and (2.7). There exists yet another conserved quantity, introduced as a Hamiltonian in [20] and derived in [5] for ribbons. It is defined through a Legendre transformation W_{Leg} of the strain energy W_S

$$\left.\begin{aligned} &W^\star(m_2, m_3, u_2, u_3) = m_2\, u_2 + m_3\, u_3 - W_S\,(u_2, u_3)\\ &W_{\mathrm{Leg}}(m_2, m_3) = \sup_{u_2, u_3} W^\star(m_2, m_3, u_2, u_3)\\ \text{and}\quad &H(n, m) = W_{\mathrm{Leg}}(m_2, m_3) + n_3. \end{aligned}\right\} \tag{7.1}$$

The Hamiltonian H is a conserved quantity: it satisfies $\mathrm{d}H/\mathrm{d}s = 0$ for any s, when evaluated on an equilibrium solution. In the equations above, $n_i = \boldsymbol{n} \cdot \boldsymbol{d}_i$, and $m_i = \boldsymbol{m} \cdot \boldsymbol{d}_i$ denote the components of the internal force and moment in the directors basis.

In equation (7.1), we consider the case where the supremum over (u_2, u_3) is attained, i.e. it is a maximum of $W^\star$: this implies that $\partial W^\star/\partial u_2 = 0$ and $\partial\, W^\star/\partial\, u_3 = 0$, which yields exactly the constitutive relations (2.4) and (2.5). As discussed in §3, for every value of (m_2, m_3), there are two corresponding solutions (u_2, u_3) by the constitutive relations; this leads to the two sheets in the three-dimensional plots. The solution set (u_2, u_3) that actually achieves the maximum in (7.1) is precisely that given by (4.3) and (4.4). We can then explicitly calculate W_{Leg} and find

$$W_{\mathrm{Leg}}(m_2, m_3) = \frac{1}{8}\left(\sqrt{m_2^2} + \sqrt{m_2^2 + m_3^2}\right)^2. \tag{7.2}$$

Downloaded from https://royalsocietypublishing.org/ on 17 November 2021

In terms of u_2 and u_3, this quantity evaluates to $W_{\mathrm{Leg}} = \frac{1}{2}\, u_2^2\, (1 + (u_3^2/u_2^2))^2 = W_S$, as noticed in [5]. Equation (7.2) corresponds to choosing a plus sign in [C.14] of [13].

For the Möbius solution from §5, for instance, we find the value of the invariant to be $H = 57.5$.

8. Conclusion

We have shown that the two main issues associated with Sadowsky's model for elastic ribbons, namely, the differential algebraic nature of the equilibrium equations and the singularity arising at inflection points ($u_2(s) = 0$) can both be overcome by using a regularized and inverted constitutive relation. We have illustrated our approach on the Möbius configuration, and have shown that the regularized model converges towards Sadowsky's model when the regularization parameter goes to zero. We note that other ways to regularize Sadowsky's equations have been used [21] but they only postpone the occurrence of the singularity that eventually arises for large enough strain. We have compared the equilibrium solution found with our model with the solution found with Wunderlich's model and we have shown that they only differ in the region where the singularity occurs: in Wunderlich's model the twist strain (u_3) is forced to vanish at the singular point (where $u_2 \to 0$) in order to leave the ratio $\eta(s) = u_3(s)/u_2(s)$ finite, while this is not the case in our approach. Besides, equilibrium equations in Wunderlich's model comprise a differential equation for the ratio $\eta(s)$ that can prove delicate to handle numerically: see for example [4] where a special fix has been introduced to lessen the numerical stiffness and be able to cross the singular event. By contrast, our approach has no such difficulties and crossing singular points is easy. In future work, it will be interesting to analyse equilibria featuring multiple singularities [16,17] and singularities for ribbons possessing natural curvature [18] using our model.

Data accessibility. This article has no additional data.

Authors' contributions. S.N. and B.A.: design, computations, analysis and writing.

Competing interests. We declare we have no competing interests.

Funding. No funding has been received for this article.

Acknowledgements. It is a pleasure to thank G. van der Heijden for providing numerical data for solutions with Wunderlich's model, as well as G. van der Heijden and A. Borum for providing feedback on the manuscript.

Appendix A. Statics in components form

The differential equations (3.1*a*) governing the equilibrium can be spelled out in components as

$$\left.\begin{aligned}
x' &= d_{3x} \quad & n_1' &= n_2\, u_3 - n_3\, u_2 \\
y' &= d_{3y} \quad & n_2' &= n_3\, u_1 - n_1\, u_3 \\
z' &= d_{3z} \quad & n_3' &= n_1\, u_2 - n_2\, u_1 \\
d_{3x}' &= u_2\, d_{1x} - u_1\, d_{2x} \quad & m_1' &= m_2\, u_3 - m_3\, u_2 + n_2 \\
d_{3y}' &= u_2\, d_{1y} - u_1\, d_{2y} \quad & m_2' &= m_3\, u_1 - m_1\, u_3 - n_1 \\
d_{3z}' &= u_2\, d_{1z} - u_1\, d_{2z} \quad & m_3' &= m_1\, u_2 - m_2\, u_1 \\
d_{1x}' &= u_3\, d_{2x} - u_2\, d_{3x} \quad & d_{2x}' &= u_1\, d_{3x} - u_3\, d_{1x} \\
d_{1y}' &= u_3\, d_{2y} - u_2\, d_{3y} \quad & d_{2y}' &= u_1\, d_{3y} - u_3\, d_{1y} \\
\text{and} \quad d_{1z}' &= u_3\, d_{2z} - u_2\, d_{3z} \quad & d_{2z}' &= u_1\, d_{3z} - u_3\, d_{1z}.
\end{aligned}\right\} \tag{A 1}$$

As explained in §3,

— for classical Kirchhoff rods, the inverse constitutive relations $u_i(s) = m_i(s)/B_i$ can be inserted directly, which yields an ODE of order 18;

Downloaded from https://royalsocietypublishing.org/ on 17 November 2021

— for a Sadowsky ribbon, one option is to complement these equations with the three constitutive relations (2.3)–(2.5), which yields a DAE with 21 unknowns.

Appendix B. Multi-valued inversion

After some algebra, the constitutive relations (2.4)–(2.5) can be inverted as

$$u_2(m_2, m_3) = \frac{\chi}{4} \frac{m_3^4 \sqrt{m_2^2 + m_3^2}}{\left(m_2^2 + m_3^2 + m_2\, \chi \sqrt{m_2^2 + m_3^2}\right)^2} \tag{B 1a}$$

and

$$u_3(m_2, m_3) = \frac{1}{4} \frac{m_3^3}{m_2^2 + m_3^2 + m_2\, \chi \sqrt{m_2^2 + m_3^2}}, \tag{B 1b}$$

where $\chi = \pm 1 = \mathrm{sign}(u_2(s=0))$. See also [13] for alternate, equivalent expressions.

The plot in figure 2 has been generated as a parametric plot, as explained in the legend, but it is also possible to generate it using the formulas above: the existence of two sheets corresponds to the choice of $\chi = \pm 1$ in the formulas above.

Appendix C. Homotopy from rods to ribbons

We use the homotopy coefficient $\rho \in (0;1)$ and replace $\lambda^\star$ with $\rho\,\lambda^\star$ in (4.3) and (4.4) to continuously pass from a rod model (having $B_1 = \infty$, $B_2 = 1$ and $B_3 = 2$) to a ribbon model

$$\left.\begin{aligned} u_2^\star(m_2, m_3, \varepsilon, \rho) &= \frac{m_2}{(1 - \rho\,(\lambda^\star - \varepsilon))\,(1 + \rho\,\lambda^\star)} \\ \text{and} \qquad u_3^\star(m_2, m_3, \rho) &= \frac{m_3}{2\,(1 + \rho\,\lambda^\star)} \end{aligned}\right\} \tag{C 1}$$

with $\rho = 0$ for rods, and $\rho = 1$ for ribbons.

References

1. Hinz DF, Fried E. 2015 Translation of Michael Sadowsky's Paper "The differential equations of the Möbius Band". *J. Elast.* **119**, 19–22. (doi:10.1007/978-94-017-7300-3_4)
2. Starostin EL, van der Heijden GHM. 2007 The shape of a Moebius strip. *Nat. Mater.* **6**, 563–567. (doi:10.1038/nmat1929)
3. Fosdick R, Fried E (eds). 2015 *The mechanics of ribbons and moebius bands*. Berlin, Germany: Springer.
4. Moore A, Healey T. 2018 Computation of elastic equilibria of complete Möbius bands and their stability. *Math. Mech. Solids* **24**, 939–967. (doi:10.1177/1081286518761789)
5. Starostin EL, van der Heijden GHM. 2015 Equilibrium shapes with stress localisation for inextensible elastic Möbius and other strips. *J. Elast.* **119**, 67–112. (doi:10.1007/s10659-014-9495-0)
6. Dias MA, Audoly B. 2015 'Wunderlich, meet Kirchhoff': a general and unified description of elastic ribbons and thin rods. *J. Elast.* **119**, 49–66. (doi:10.1007/s10659-014-9487-0)
7. Audoly B, Seffen KA. 2015 Buckling of naturally curved elastic strips: the ribbon model makes a difference. *J. Elast.* **119**, 293–320. (doi:10.1007/s10659-015-9520-y)
8. Moulton DE, Grandgeorge P, Neukirch S. 2018 Stable elastic knots with no self-contact. *J. Mech. Phys. Solids* **116**, 33–53. (doi:10.1016/j.jmps.2018.03.019)
9. Kumar A, Handral P, Bhandari D, Rangarajan R. 2021 More views of a one-sided surface: mechanical models and stereo vision techniques for Möbius strips. *Proc. R. Soc. A* **477**, 20210076. (doi:10.1098/rspa.2021.0076)
10. Freddi L, Hornung P, Mora M-G, Paroni R. 2015 A corrected Sadowsky functional for inextensible elastic ribbons. *J. Elast.* **123**, 125–136. (doi:10.1007/s10659-015-9551-4)

11. Paroni R, Tomassetti G. 2019 Macroscopic and microscopic behavior of narrow elastic ribbons. *J. Elast.* **135**, 409–433. (doi:10.1007/s10659-018-09712-w)
12. Audoly B, Neukirch S. 2021 A one-dimensional model for elastic ribbons: a little stretching makes a big difference. *J. Mech. Phys. Solids* **153**, 104457. (doi:10.1016/j.jmps.2021.104457)
13. Borum A. 2018 Manipulation and mechanics of thin elastic objects. PhD thesis, University of Illinois at Urbana-Champaign.
14. Domokos G, Healey T. 2001 Hidden symmetry of global solutions in twisted elastic rings. *J. Nonlinear Sci.* **11**, 47–67. (doi:10.1007/s003320010008)
15. Mahadevan L, Keller JB. 1993 The shape of a Möbius band. *Proc. R. Soc. Lond. A.* **440**, 149–162. (doi:10.1098/rspa.1993.0009)
16. Yu T, Hanna JA. 2019 Bifurcations of buckled, clamped anisotropic rods and thin bands under lateral end translations. *J. Mech. Phys. Solids* **122**, 657–685. (doi:10.1016/j.jmps.2018.01.015)
17. Huang W, Wang Y, Li X, Jawed MK. 2020 Shear induced supercritical pitchfork bifurcation of pre-buckled bands, from narrow strips to wide plates. *J. Mech. Phys. Solids* **145**, 104168. (doi:10.1016/j.jmps.2020.104168)
18. Charrondière R, Bertails-Descoubes F, Neukirch S, Romero V. 2020 Numerical modeling of inextensible elastic ribbons with curvature-based elements. *Comput. Methods Appl. Mech. Eng.* **364**, 112922. (doi:10.1016/j.cma.2020.112922)
19. Todres RE. 2015 Translation of W. Wunderlich's "On a Developable Möbius Band". *J. Elast.* **119**, 23–34. (doi:10.1007/978-94-017-7300-3_5)
20. Kehrbaum S, Maddocks JH. 1997 Elastic rods, rigid bodies, quaternions and the last quadrature. *Phil. Trans. R. Soc. Lond. A* **355**, 2117–2136. (doi:10.1098/rsta.1997.0113)
21. Sano TG, Wada H. 2019 Twist-induced snapping in a bent elastic rod and ribbon. *Phys. Rev. Lett.* **122**, 114301. (doi:10.1103/PhysRevLett.122.114301)

Downloaded from https://royalsocietypublishing.org/ on 17 November 2021